THREE-DIMENSIONAL LIMIT ANALYSIS OF THE VICOFORTE ELLIPTICAL DOME

Giulio Ventura(1*), Marco Coppola(2), Chiara Calderini(3) and Mario Alberto Chiorino(4)

(1) Politecnico di Torino, Department of Structural and Geotechnical Engineering, Corso Duca degli Abruzzi 24, 10129 Italy. Ph. +390110904906, E-Mail: giulio.ventura@polito.it

(2) Politecnico di Torino, Department of Structural and Geotechnical Engineering, Corso Duca degli Abruzzi 24, 10129 Italy. Ph. +393280125432, E-Mail: marco.coppola@studenti.polito.it

(3) Università di Genova, Dipartimento di Ingegneria delle Costruzioni, dell'Ambiente e del Territorio, Via Montallegro 1, 16145 Genova, Italy, E-Mail: chiara.calderini@unige.it

(4) Politecnico di Torino, Department of Structural and Geotechnical Engineering, Corso Duca degli Abruzzi 24, 10129 Italy. Ph. +390110904864, E-Mail: mario.chiorino@polito.it

(*) Corresponding Author.

Abstract

Limit Analysis provides a conceptually simple and robust method to estimate the safety of structures and has been long applied to the analysis of the ultimate collapse state of two-dimensional masonry structures or structural elements. In revolving symmetric domes, the three-dimensional problem can be reduced to the two-dimensional case under appropriate hypotheses. The Vicoforte dome is the largest elliptical dome in the world, and its complex geometry makes this kind of analysis not straightforward. Starting from some basic assumptions, a method for analyzing the three-dimensional elliptical geometry and understand the behavior at collapse of the drum-dome system using limit analysis is proposed. The three dimensional collapse mechanism is found and the system behavior including the presence of tension rings at different levels is interpreted. The results are compared against a nonlinear finite element model.

Keywords: Three-dimensional Limit Analysis, elliptical masonry dome, tension ring, kinematic theorem, virtual work.

1 INTRODUCTION

The dome of the Sanctuary of Vicoforte is, with its 38.15 m of major axis and 24.80 m of minor axis, the biggest elliptical dome in the world, Figure 1, Figure 2. Erected in 1732, the Sanctuary was affected by differential settlements of the foundation since the beginning of its construction, due to the poor quality of the soil at the site. This led to several and significant structural problems to the drum-dome system, exhibited by an extended network of cracks along the meridian directions.

For this reason, the Italian Ministry of Cultural Heritage financed in 1975 some studies on the structure and the foundations (mainly focused in investigating the nature of the supporting soil), a topographic survey and investigations on the masonry and crack network. These analyses were performed by the company Rodio and the Engineers Bernasconi and Marchini (Bernasconi and Marchini, 1979), while Politecnico di Torino determined by experimental tests the physical and mechanical properties of the masonry. More recent studies and the problem of modeling and monitoring the Vicoforte dome can be found in (Chiorino et al., 2006, 2008).

The potential of the application of plastic limit analysis to the estimation of the safety of masonry structures is well known. Its principles have been established by Kooharian (Kooharian, 1953) and Heyman (Heyman, 1966, 1988) in their pioneering works, although first traces and applications of the method are far older and are related to the restoration of St. Peter’s dome, as reported in the works by Hooke (Hooke, 1675) and Poleni (Poleni, 1748). Recent review papers on the method and on new advanced modeling techniques are (Gilbert, 2007; Huerta, 2008; Roca *et al.*, 2010).

The application of limit analysis to masonry considers the material as rigid, with unlimited strength in compression and without tensile strength. Consequently, the stability is the major relevant criterion to analyze the ultimate state of collapse, in the sense of the geometrical factor of safety concept introduced in (Heyman, 1988).

To present the methodology used in this paper, we recall that the application of limit analysis theorems to masonry is based on the static or kinematic approaches (like in plasticity). The static approach is based on verifying that the geometry of the structure is able, with a certain safety margin, to carry the loads to the ground without tensile stresses in the structure, i.e. on finding a thrust line which stays everywhere "sufficiently" inside the masonry structural elements, (Heyman, 1988). For a masonry arch, the static (safe) theorem guarantees that, if it is possible to find a thrust line in equilibrium with external load and self weight internal to the cross sections of the arch, the arch is safe. In masonry domes, the problem can be treated in the same quasi-two-dimension case, if we admit the development of cracks in the direction of the meridians and the consequent subdivision in "orange-slice" arches. This method was used by Poleni (Poleni, 1748) to assess the safety of St. Peter dome in Rome and plan the subsequent restoration works. The other approach is through the kinematic or upper bound theorem and is based on finding the collapse mechanism corresponding to the minimum load multiplier and associated to a positive work of the loads. Since in many cases self-weight is the most important loadcase in masonry structures, once a mechanism is fixed, the weights (in general the loads) are subdivided in "pushing" (i.e. producing positive virtual work in the mechanism) and "resisting" (i.e. producing negative virtual work in the mechanism) and the absolute value ratio between positive and negative work is assumed as a safety coefficient for the structure. Moreover, when the kinematic theorem is used, an upper bound of the safety coefficient for the structure is obtained. It will coincide with the true safety factor only when the assumed collapse mechanism coincides with the real one. Therefore, it is important to assume appropriately the collapse mechanism and vary the position of the mechanism hinges so that the minimum safety coefficient is found.

The tensile contribution of circumferential steel ties, often used as reinforcement in masonry domes, can be taken into account by adding their plastic dissipation work, caused by circumferential deformation of the rings in the development of the mechanism (Como, 1997). This type of approach has been used in the limit analysis of the dome of Vicoforte (Reffo, 2002; Chiorino *et al*., 2006), extending the method used for domes of revolution to the elliptical dome of Vicoforte by considering the two extreme cases of slices cut in correspondence with the major and minor axes.

However, the elliptical dome of Vicoforte, can be conceptually divided into infinite "orange-slice" arches, each one of different geometry and with its own ideal collapse mechanism and safety coefficient. Moreover, all these ideal arches are mutually constrained by the circumferential ties, i.e. bound together in a global three dimensional mechanism. Furthermore, the circumferential ties, called in the following tension rings, do not necessarily have the same stress levels because, being positioned at different heights, they have different radial displacement, strain and stress level in the mechanism. Finally, depending on tie-masonry bond strength, the stress state may vary from point to point in the ring.

In this paper, a simple method is introduced for analyzing the three dimensional collapse mechanism of the elliptical dome and to estimate the global safety coefficient. The analysis will include the influence of the circumferential ties in different hypotheses. The paper is structured as follows: in Section 2, the geometry of the dome is analyzed, its discretization is defined and the general form of the dissipation work at the tension rings is given. Section 3 presents the stability analyses for the single slices and the global 3D mechanism with and without the contribution of the tension rings. Section 4 extends the analysis to the case of rings with limited maximum elongation to assess the effectiveness of the tension rings position and cross section area. Finally, Section 5 compares the results of the proposed method to the results of a much more sophisticated finite element model, published in (Calderini *et al*., 2006; Chiorino *et al*., 2008), and here adapted to evaluate the limit multiplier of the self-weight.

2 KINEMATIC 3D LIMIT ANALYSIS

2.1 The geometric model

The application of limit analysis requires, as pointed out in the previous Section, identifying the proper collapse mechanism by dividing the dome slices into rigid blocks whose weight produces virtual work in the mechanism. As the hinges of the mechanism are to be varied to determine the minimum safety coefficient, an important problem is how to evaluate the weight and center of mass of the rigid blocks in which each slice is subdivided up to a reasonable approximation. In general, this evaluation can be not straightforward due to the architectonical features of the dome.

To this end, a simplified solid model of the drum-dome has been defined, as an accurate and detailed model is unnecessary for the purpose of the global stability analysis addressed in the present work, Figure 3. In fact, the stability assessment of the dome involves the use of loads of large order of magnitude given by the self weights of the ideal rigid blocks. A complex geometric reconstruction would not improve significantly the approximation of the numeric computation of the minimum safety coefficient. Therefore, as the observed state of the structure suggests, the dome was divided into sixteen slices and a collapse mechanism was associated to each one, idealized with a cross section passing through its centerline. Because of symmetry, there are only four slices to be analyzed, Figure 4. For each slice, the kinematic arbitrary parameter of the mechanism is the lantern virtual vertical displacement η, that is assumed equal for all slices.

The typical mechanism of collapse of a drum-dome half arch is characterized by three hinges, placed alternatively at the extrados and at the intrados, Figure 5. Such subdivision identifies the rigid blocks in relative rotation to each other. The crack network and all the literature on Vicoforte dome suggest that the potential failure mechanism involves the entire drum-dome system. We assume that, for symmetry reasons, the skylight lantern has only vertical translation, so it can be considered as a weight applied at the top of the slices. The hinge at the drum base and the one at the top of the dome can be assumed as fixed, whereas the hinge at intrados (C_2) is variable, and its position will be determined to find the most critical mechanism, i.e. the mechanism for which the safety factor is minimum. In between the hinges, the structure is assumed as one rigid block. Each block is characterized by its volume and centroid and let α be the angle of the intrados hinge position. The volume and centroid position has been geometrically computed at several discrete values of α, Figure 6. Then, for every slice, a volume function of α was defined by polynomial data approximation. These functions represent the volume of each slice under the ray with angle α. By computing the difference to the total volume of the slice, the volume function for the complementary part (between the uppermost hinge and the center C_2) is immediately obtained. Likewise, polynomial data approximations for the first moments of area of the rigid blocks above and below the center C_2 have been defined as well. These polynomial functions allow to determine the center of mass of the two rigid blocks above and below the variable hinge as a function of its position, given by the angle α. All the relevant polynomial functions are reported in Tables 1,2,3. Assuming a unit weight for the masonry equal to 17.0 $\mathrm{kN/m^3}$ (determined by experimental testing at the Politecnico di Torino for the analyses of Bernasconi and Marchini in 1976) and evaluating the mechanism virtual displacements at the centroids, the virtual works of the rigid blocks can be immediately computed and the ratio W_r/W_p, between resisting (W_r) and pushing (W_p) work, is evaluated as function of α for each dome slice. Of course, a distinct angle α for each slice has been considered. In fact, the correct position of the intermediate hinge may vary in each slice, as the curvature of the slices differs. Then, an iterative procedure has been developed to find the minimum ratio between resisting and pushing work and, consequently, the position of the intermediate hinge in each slice of the dome. The details of the simulations will be given in Section 3.

2.2 The work of the tension rings

The stability of a dome is usually ensured by placing tension rings at different heights. In the dome of Vicoforte three original iron rings are present. With reference to Figure 7, rings 1 and 2 have a cross section area of 5600 mm^2, ring 3 has a cross section area of 2750 mm^2 and the iron yield strength σ_0, in a rigid plastic model, can be assumed equal to 167 MPa (Chiorino *et al*., 2006; Reffo, 2002).

The contribution to the stability given by the presence of the original iron rings is then considered. Let R be the radius of curvature and δ_r the radial displacement at a point, then the consequent circular strain is given by

$$\varepsilon_\phi = \delta_r / R \tag{EQ1}$$

where ϕ is the polar angle spanning the horizontal plane. Similarly to the case of circular domes (Como, 1997), we can evaluate the tension ring resisting plastic work by integration in between the two angles ϕ_1 and ϕ_2 subtending a slice:

$$W_t = A_r \int_{\phi_1}^{\phi_2} \sigma_0 \varepsilon_\phi R \, \mathrm{d}\phi = A_r \sigma_0 \int_{\phi_1}^{\phi_2} \delta_r \, \mathrm{d}\phi \tag{EQ2}$$

Let $\Delta\phi = \phi_2 - \phi_1$. Assuming a constant radial displacement δ_r at each point of the slice it is:

$$W_t = \sigma_0 A_r \Delta\phi \, \delta_r \tag{EQ3}$$

From the kinematics of the slice, Figure 5, the radial displacement δ_r is immediately determined as the horizontal displacement at the height where the tension ring is positioned. Therefore, the resisting work of each tension ring can be calculated as the sum of the work at each slice and the total resisting work as the sum of the work at each tension ring.

3 THE STABILITY COMPUTATION OF THE DOME

3.1 Stability of the dome without tension rings

We imagine in this case that each dome slice behaves independently, with its own geometry. For each slice the intermediate hinge position is determined by minimizing the ratio between the slice resisting and pushing works. Table 4 lists the obtained results both in term of hinge position (angle α, Figure 6) and as resisting/pushing work ratio. The most critical part of the dome is slice A with a safety coefficient $(W_r/W_p)_{\text{Slice A}} = 0.79$. This slice is at the maximum dome diameter, Figure 4. In Figure 8(a) the work ratio in slice A is plotted as function of the hinge position α. It shows an unique minimum at α = 0.6226 radians, which corresponds to 35°38'. The determined position is therefore a global minimum for the work ratio.

From the results reported in Table 4 it can be observed that the safety coefficient varies significantly from slice to slice and in two slices (A and D) the equilibrium of the dome without tension rings is impossible. Of course, slices B and C benefit from the presence of the buttresses, so that their safety coefficient is much higher.

In the above computation the minimization of the ratio W_r/W_p has been done independently for each slice. On the other hand, even if tension rings are assumed not to be present, it can be imagined that the more stable slices sustain somehow the adjacent unstable ones or other load paths are created. This can be approximated by adding the contribution of each slice to W_r and W_p, obtaining a work ratio function of four variables to be minimized. The value of the variables at the solution will give the new position of the mechanism hinges in this hypothesis. These are reported in Table 5 and the global safety coefficient becomes

$$\left(\frac{W_r}{W_p}\right)_{Dome} = 1.27 \qquad \text{(EQ4)}$$

Therefore, with this assumption the equilibrium of the dome is possible, although the safety coefficient is not very high and the less stable parts, especially slice A, may determine collapse.

It is interesting to observe how the hinge positions vary when the dome is considered as an unique system instead of being analyzed by single slices. In single slice analysis, the more stable slices show a higher position of the intermediate hinge (compared to the least stable slices). When the global mechanism is considered, the hinge position of the unstable slices is raised, giving a higher overall stability.

3.2 Stability of the dome including tension rings

In this Section, the stability of the dome is analyzed considering the contribution of the tension rings both in the case of independent slices and in the case of a global mechanism. Here, the usual hypothesis of complete plasticization of the rings will be adopted, so that each point of the rings will be subjected to a tensile stress equal to the yield strength σ_0 and the relevant resisting work in the collapse mechanism is taken into account. No upper limit to ring elongation will be considered. This hypothesis will be removed in Section 4.

In Table 6, each slice mechanism is considered as independent and the intermediate hinge positions have been determined by minimizing the ratios between the resisting and pushing work of each slice. All the slices of the dome present high W_r/W_p ratios and the intermediate hinge positions are now higher, their angles being in between 42° and 47°.

When all the slices are considered part of a global mechanism, so that the global ratio of resisting to pushing work is minimized, the safety coefficient is found to be:

$$\left(\frac{W_r}{W_p}\right)_{Dome} = 3.03 \qquad \text{(EQ5)}$$

In Table 7, the results for the intermediate hinge positions in this case are reported. The global static stability of the dome in this hypothesis is high. This hypothesis is the closest to the real situation provided that all tension rings can yield simultaneously. This hypothesis will be removed in the next Section introducing the steel limit tensile strain.

Compared to the solution of Table 5 (dome without tension rings), the presence of the rings raises the intermediate hinge positions. This can be immediately observed comparing Figure 8(a) and (b), where the work ratio is plotted against the hinge position for the slice A without (a) and with (b) tension rings contribution, showing a shift of the minimum point toward higher angles.

4 TENSION RINGS WITH LIMITED ELONGATION

4.1 Limit analysis and the maximum deformation of the tension rings

Limit analysis is based on the hypothesis of perfectly plastic materials, i.e. no upper bound to plastic deformation is introduced, and this simplification is acceptable in many engineering problems and applications to metal structures or structural components. The translation of this theory to masonry and block structures is nowadays standard practice and limit analysis plays a major role in the assessment of existing masonry and monumental buildings. However, especially for tension rings in domes, the hypothesis that for the assumed mechanism plasticization can be complete at all points is not conservative and may be incorrect. In fact, some observations concerning the plastic dissipation work of the tension rings are necessary to avoid overestimation of their resisting work. Note that, as the tension rings are positioned at different heights, they will be subjected to different axial strains $\varepsilon_\phi = \delta_r / R$ depending on the different radial displacement and curvature radius of each tension ring. Let us introduce the hypothesis that the tension rings have an elastic-plastic constitutive law with limited tensile elongation. From literature data, the steel yielding stress σ_0 is 167 MPa (Chiorino *et al*., 2006; Reffo, 2002; Bussell, 1997), and the elastic modulus E can be assumed equal to 200 GPa. Consequently, the yield strain is $\varepsilon_y = \frac{\sigma_0}{E} = 8 \cdot 10^{-4}$ while the elongation at failure ε_u of wrought iron can be given a conservative value of 7% (Bussell, 1997), i.e. $\varepsilon_u = 7 \cdot 10^{-2}$.

Denote with ε_i the strain at the i^{th} tension ring $(i = 1 \dots 3)$ and let $\varepsilon_{\max} = \max(\varepsilon_1,\ \varepsilon_2,\ \varepsilon_3)$, $\varepsilon_{\min} = \min(\varepsilon_1,\ \varepsilon_2,\ \varepsilon_3)$. Then, the three tension rings can exhibit simultaneously plastic dissipation work if the difference of the maximum to the minimum strain is less than the extension of the plastic plateau, i.e. if $\varepsilon_{\max} - \varepsilon_{\min} \leq \varepsilon_u - \varepsilon_y$. To better explain this concept, assume, without loss of generality, that $\varepsilon_1 < \varepsilon_2 < \varepsilon_3$ and that the kinematic arbitrary parameter of the mechanism is the lantern virtual vertical displacement η. Then, the mechanism's horizontal displacements will be proportional to η, as well as the tension ring strains. Imagine to increase the arbitrary mechanism parameter η. For low values of η, all the ε_i will be in the elastic range and the rings can be considered as elastic constraints. Then, as η increases, first the tension ring of maximum strain, then all the others, will enter the plastic range. The strain can increase up to the limiting value ε_u, at which the ring will break and its stress will drop to zero, Figure 9. Therefore, before considering the plastic dissipation contribution of all the tension rings, it must be verified that their elongation is compatible with their ultimate strain, i.e. that $\varepsilon_{\max} - \varepsilon_{\min} \leq \varepsilon_u - \varepsilon_y$. If not, the above analysis allows to determine their breaking sequence and their effective contribution to the "resisting" virtual work. Therefore, a simple method is described in the following to perform this task.

Suppose the collapse safety factor at the breaking of the most strained tension ring is to be evaluated. Given an arbitrary initial mechanism parameter η_0, the ratio $k_0 = \varepsilon_u/\varepsilon_{max}$ between the ultimate (breaking) strain and the maximum strain at the tension rings is defined. Then the mechanism parameter is set as $\eta_1 = k_0\eta_0$, i.e. in such a way that $\varepsilon_{max} = \varepsilon_u$. The strain and stresses in the other tension rings are evaluated assuming the elastic-plastic constitutive law previously defined and considering in the analysis the relevant forces and resisting work. In this way, a first structural safety coefficient s_1 is determined. Then, the broken tension ring is discarded and the analysis is repeated in the same way with the remaining two, determining a second structural safety coefficient s_2. Finally, only the third tension ring is considered and a third structural safety coefficient s_3 is obtained. Depending on the size and on the arrangement of the tension rings in the dome, it is not necessarily so that $s_1 \geq s_2 \geq s_3$, but the global structural safety coefficient is $s = \max\,(s_1, s_2, s_3)$.

A final issue about the behavior of the tension rings concerns the effective strain distribution along their length. We can imagine two limiting situations. In the first, the strain (and therefore the stress) is constant along the ring. This physically corresponds to no friction between masonry and the tension ring. In the second, the tension ring is imagined "glued" to the masonry, so that no slip is allowed between masonry and the tension ring. This means that strain and stresses may vary along the ring. In the following, when this hypothesis will be taken into account, a piecewise constant stress for each ring and dome slice will be assumed.

The real situation will be in between these two limiting cases, that will be both analyzed.

4.2 Limit analysis for limited tension rings elongation

The case of uniform strain in each tension ring will be analyzed first. In this case, as specified in the previous section, the strain and stress is assumed as constant in each tension ring. Following the method illustrated in Section 4.1, we set the mechanism's kinematic parameter (lantern vertical displacement η) so that the maximum strain in the rings is equal to $\varepsilon_u = 7 \cdot 10^{-2}$. The other rings are automatically shifted at minor strain. In Table 8, the strains in the rings are shown in this hypothesis and it is

$$\varepsilon_{\max} - \varepsilon_{\min} = 2.4 \cdot 10^{-2} \leq \varepsilon_u - \varepsilon_y = 7 \cdot 10^{-2} - 8 \cdot 10^{-4} = 6.92\ 10^{-2} \qquad \text{(EQ6)}$$

Therefore, being the difference $\varepsilon_{\max} - \varepsilon_{\min}$ smaller than the extension of the plastic plateau (given by the difference $\varepsilon_u - \varepsilon_y$, Figure 9), Equation (6), we can conclude that the rings are well positioned: the range between the maximum and the minimum strain in the rings in this case is about 35% of the length of the steel plastic plateau. They will be all able of entering the plastic regime without a premature breaking of the most strained. In particular, it can be computed that all the rings will enter the plastic regime at a lantern vertical displacement of 31 cm, while the most strained ring will break for a lantern vertical displacement of 88.6 cm. On the other hand, a very short steel plastic plateau or not efficient ring positions can lead to cases where the rings cannot enter simultaneously the plastic regime, so that their resisting work cannot be fully exploited.

Note that, although the assumed value for the strain at failure is not supported by experimental tests, the absolute minimum for wrought iron elongation at failure found in the literature is 4%, so that the present hypothesis of uniform strain in the tension rings with simultaneous plasticization is valid being, according to Equation (6), $\varepsilon_{\max} - \varepsilon_{\min} = 2.4 \cdot 10^{-2} < 4.0\ 10^{-2}$.

Finally, the influence of a possible uneven distribution of strain-stress in steel rings is considered. This situation can arise both because the iron is tied by friction and adherence to the masonry and because, in an event of collapse, the relative speed of the phenomenon can forbid a uniform redistribution of the stress in the rings, so that their plastic resources cannot be fully available.

To model this situation, an approach, conceptually equal to the one presented in Section 4.1, has been used. However, to account for the uneven strain distribution, the elongation in the rings has been computed at the level of the single slice, and considered as independent from slice to slice. In this way, each ring presents piecewise constant strain function of the radial displacement and curvature radius, Equation (1).

In Table 9, the strain states are shown for a mechanism parameter (lantern displacement) such that the maximum strain is equal to $\varepsilon_u = 7\%$. The maximum strain takes place in the tension ring 1, slice A, due to lower position of the hinge and consequently the greater radial displacement associated to the mechanism, see Table 6, and the predicted lantern vertical displacement for this mechanism is 77.7 cm. In this case, the steel's plastic range required by the structure is $\varepsilon_{\max} - \varepsilon_{\min} = 0.070 - 0.034 = 3.60\ 10^{-2}$, i.e. about 51% of the assumed limit ($\varepsilon_u = 7 \cdot 10^{-2}$). If the iron of the dome would have particularly low elongation at failure, then breaking of the most strained tension ring may be possible before tension ring 3 entering the plastic regime (we recall that the minimum literature wrought iron elongation at failure is 4%). For this phenomenon not to occur the elongation at failure must be greater than $\varepsilon_{\max} - \varepsilon_{\min} + \varepsilon_{\mathrm{y}} = 3.68\%$.

The lantern vertical displacement for the two examined cases may appear very large. However, this is due to the fact that the largest part of the displacement is not generated when the tension rings are in the elastic range, but in the long horizontal plastic plateau. In fact, we recall that the yield strain is $8 \cdot 10^{-4}$ while the ultimate strain is $7 \cdot 10^{-2}$, i.e. nearly 100 times larger. If we think not to use the steel's plastic resources and to find the displacement η_y that brings the most strained ring at yielding, we find $\eta_y = 1$ cm and the strain-stress state in the rings is shown in Table 10. As the rings are now all (except the yielded one) in the elastic range, the stability ratio is now changed and it is

$$\left(\frac{W_r}{W_p}\right)_y = 2.08 \qquad \text{(EQ7)}$$

5 NON-LINEAR INCREMENTAL ANALYSIS

In order to assess the results of the proposed method, non-linear static incremental analyses of the dome-drum system under gravity loads have been performed. The FEM model of the structure is depicted in Figure 10. The dome is modeled by non-linear orthotropic shell elements, the vault being defined by the mean surface and the masonry pattern being described by element reference systems rotated according to the actual orientation of mortar joints. The lantern is not included in the model, but its weight is applied to the top masonry ring of the dome as a surface load. The iron rings are modeled by non-linear link elements for which a Von Mises strength criterion is adopted. For the masonry, the non-linear constitutive law defined in (Calderini and Lagomarsino, 2008) and implemented in a general-purpose finite element code (ANSYS, 2003) is applied. In particular, 4-node non-linear shell elements with five integration points through the thickness (thus describing the out-of-plane behavior besides the in-plane one) are used. The mechanical parameters adopted are summarized in

Table 11. Except for the compressive strength of the masonry and Young's modulus (Barosso, 1979), all the parameters have been defined qualitatively by considering the values typically associated with historic masonry (Binda, 1996). It has been assessed through a set of non-linear analyses that, in a reasonable range of parameter values, the response of the structure is not pathologically influenced by the variability of the parameters. This model and the relevant discussion has been published in (Calderini *et al*., 2006) and (Chiorino *et al*., 2008). Here the model is used for computing the multiplier of the self weight at collapse for the sake of comparison to the limit analysis results obtained with the proposed methodology.

Two different constraining configurations are considered. In the first one (named VD), the model is constrained by inhibiting the vertical displacements only of all the nodes at the base of the drum (global rigid motions are inhibited by constraining all the degrees of freedom of one single node); this is a limit configuration in which it is assumed that the retaining stiffness contribution of the structure lying under the drum is null. In the second (named VHD), both vertical and horizontal displacements of all the nodes at the base of the drum are inhibited; this is an opposite limit configuration in which the structure lying under the drum is considered as infinitely stiff. It is well evident that the actual behavior of the structure is in between these two limit configurations.

The incremental analyses in the two cases have been performed by increasing the gravity loads up to collapse. In Figure 11 the force-displacement curves are represented. They have been obtained by plotting, for each load step, the load multiplier as a function of the displacement of one node at the top of the dome; convergence was lost after the last plotted point. The obtained load multiplier is 2.98 for VD and 5.39 for VHD. The collapse modes are represented in Figure 12. In Figure 13, the plastic strains normal to principal mortar joints are represented (strains are depicted only in those elements in which joints were cracked). In one case (VD), the system tends to ovalize, the transversal axis being subjected to the highest stresses and damage (the enlargement of the base of the drum in this direction is 0.148 m, while in the longitudinal one is 0.013 m). All the three rings are plasticized along the minor axis. By observing the deformed shape of the transversal section, it can be noted that the structure behave as an arch-pier system with complaining horizontal boundaries, whose stiffness is defined by stiffness and strength of the dome-drum system along its parallels (and thus by the strength of masonry in the direction of principal mortar joints). The three hinges (Figure 12, hinge scheme) are placed on the opposite side of the section with respect to limit analysis model. In the case VHD, the collapse mechanism is more similar to that considered in the limit analysis and only the two upper rings are plasticized (also in this case, along the transversal axis). The computed collapse modes confirm the mechanism assumption used in limit analysis.

The non-linear incremental analysis shows that the collapse multiplier is strongly influenced by the boundary conditions of the system. By considering the stiffness of the structure lying under the dome-drum system, it can be stated that VHD configuration is closer to reality.

By observing the sequence of limit analysis results obtained in the previous sections it can be observed that, quite naturally, the safety coefficient estimate for the dome increases as further resisting mechanisms are introduced (slices collaboration, tension rings contribution). We expect therefore that the global safety coefficient will increase as new sources of strength are added to the structure. In particular, the finite element model accounts for an additional masonry circumferential strength that is not present in the limit analysis model. In this light we explain the difference between the limit analysis estimate of a safety coefficient of about 3 and a finite element collapse load multiplier in between 3 and 5.

6 CONCLUSIONS

In the present paper a simple method for analyzing 3D dome collapse mechanisms has been presented. The method is based on the construction of nonlinear approximation functions of weights and first moments of inertia as well as non-symmetric dome collapse mechanisms. Then the analyses have been expanded to consider the ductility of the steel tension rings and a method for evaluating their correct position and cross section has been proposed. Both the cases of no friction and completely bonded tension rings have been examined and an evaluation of the lantern displacement required for the activation of each mechanism has been given. The proposed method has been applied to the elliptical dome of the Vicoforte di Mondovì Sanctuary.

Comparing the analyses results it may be observed that, as new resisting contributions are introduced, the mechanism intermediate hinge tends to shift upwards and the safety coefficients increases as well. From the analyses we have in fact:

- independent slices without tension rings: this is the weakest dome strength hypothesis with the lowest safety coefficients (collapse at two slices is predicted);
- interacting slices without tension rings: a circumferential interaction hypothesis is introduced. The safety coefficient increases (1.27) and the intermediate hinges are higher than the previous case;
- independent slices and bonded tension rings: the tension rings substantially contribute to the dome stability. The safety coefficients substantially increase (range 2.7÷3.5) and the intermediate hinges are higher than the previous case;
- interacting slices and uniformly stressed tension rings: this is similar to the previous case. The intermediate hinge positions tend to approach each other in a substantially high position and the global safety coefficient is 3.03, roughly the mean of the coefficients of the previous case.

The last two hypotheses are of course the closest to the real condition for the dome (they are the two considering the existence of the tension rings) and yield very similar stability results. Note, however, that the correct tension ring contribution can be considered only after verifying, as done in the present work, which rings are able of yielding simultaneously and which (if any) remain in the elastic range. Although the proposed method is very simple, it has proved to give conservative results compared to a much more complex and computationally expensive nonlinear finite element model.

Therefore, even if accurate modeling by the more recent techniques appear a valuable tool for limiting at most any needed intervention on the architectural heritage, the proposed limit analysis methodology seems able of giving a useful first estimate of the global safety coefficient.

7 REFERENCES

ANSYS User's Manual for Revision 8.0. 2003. ANSYS Inc., Houston, USA.

Barosso L. 1979. La struttura tamburo/cupola del Santuario: materiali e tecniche costruttive. *Atti e Rassegna Tecnica della Società degli Ingegneri e degli Architetti in Torino*, 6:269-73. Special Issue dedicated to Vicoforte Sanctuary.

Bernasconi, F. and Marchini, S. 1979. La stabilità del Santuario nelle condizioni attuali: analisi del regime statico della struttura e proposte di intervento. *Atti e Rassegna Tecnica della Società degli Ingegneri e degli Architetti in Torino*, 6:288-94. Special Issue dedicated to Vicoforte Sanctuary.

Binda, L. 1996. The knowledge of materials and construction techniques: an important step for the evaluation of masonry structures. *Proc. of the 2nd Joint USA/Italy Workshop Learning from practice: Damage assessment for design decision and effectiveness of techniques*, 3-27. Rome: CNR.

Bussell M. 1997. *Appraisal of existing iron and steel structures*. Publication 138, The Steel Construction Institute, Ascot, UK.

Brencich, A. and Morbiducci, R. 2007. Masonry arches: historical rules and modern mechanics. *International Journal of Architectural Heritage*, 1: 165-189.

Calderini, C., Chiorino, M.A., Lagomarsino, S. and Spadafora, A. 2006. Non linear modelling of the elliptical dome of Vicoforte. In *V Int. Conf. on Structural Analysis of Historical Constructions*, 1177-1186. New Dehli.

Calderini, C. and Lagomarsino, S. 2008. An anisotropic damage model for historical masonry. *Journal of Structural Engineering*, ASCE, 134(2): 209-220.

Chiorino, M.A., Roccati, R., D'Addato, C., Aoki, T., Calderini, C. and Spadafora, A. 2006. Monitoring and modeling strategies for the world's largest elliptical dome at Vicoforte. In *5th Int. Conf. on Structural Analysis of Historical Constructions.* New Dehli.

Chiorino, M.A., Spadafora, A., Calderini, C., Lagomarsino, S. 2008. Modeling Strategies for the World's Largest Elliptical Dome at Vicoforte. *International Journal of Architectural Heritage* 2: 274–303.

Como, M. 1997. Un antico restauro statico della cupola di San Pietro a Roma. In *Lo specchio del cielo*, 245-259. Edited by C. Conforti. Electa, Milan.

Gilbert, M. 2007. Limit analysis applied to masonry arch bridges: state-of-the-art and recent developments. In *ARCH07 - 5th international conference on arch bridges*, 13-28.

Heyman, J. 1966. The stone skeleton. *International Journal of Solids and Structures*, 2:249-279.

Heyman, J. 1977. *Equilibrium of shell structures*. Clarendon Press. Oxford.

Heyman, J. 1988. Poleni's problem. *Proceedings of The Institution of Civil Engineers,* 84:737-759.

Hooke, R. 1675. *A description of Helioscopes, and some other instruments*. John & Martin Printer to the Royal Society. London.

Huerta, S. 2008. The analysis of masonry architecture: A historical approach. *Architectural Science Review*, 51(4): 297-328.

Kooharian, A. 1953. Limit analysis of voussoir (segmental) and concrete arches. In *Proceedings of the American Concrete Institute*, 89: 317-328.

Mahesh Varma, N., Jangid, R. S., Achwal, V. G. 2006. Tension Ring in Masonry Domes. In *V Int. Conf. on Structural Analysis of Historical Constructions*. New Dehli.

Poleni, G. 1748. *Memorie istoriche della gran cupola del tempio vaticano e dé Danni di essa, e dé ristoramenti loro*. Padova.

Reffo, A. 2002. Limit analysis of large masonry domes: the dome of the Sanctuary of Vicoforte. *Graduation thesis*, Chiorino, M. A. tutor. School of Architecture, Politecnico di Torino.

Roca, P., Cervera, M., Gariup, G., Pelà, L. 2010. Structural Analysis of Masonry Historical Constructions. Classical and Advanced Approaches. *Archives of Computational Methods in Engineering*, 17(3): 299-325.

FIGURE CAPTIONS

Figure 1: External (left) and internal (right) views of the Sanctuary of Vicoforte.

Figure 2: A cross-section of Sanctuary (left) and cracks in the dome (right) of a east-west section, North side view (Garro 1962).

Figure 3: The three-dimensional geometric computational model.

Figure 4: The four fundamental slices. Plan view (left) and 3D view (right).

Figure 5: The mechanism in a generic slice.

Figure 6: Subdivision of a slice at discrete positions.

Figure 7: Tension ring positions.

Figure 8: The virtual works ratio vs. intermediate hinge position a in slice A without (a) and including (b) tension rings contribution.

Figure 9: Example illustration of the strain distribution in the tension rings and associated stress state according to elastic-plastic constitutive law.

Figure 10: FEM model of the dome-drum system (the model is sliced along the longitudinal axis in order to show its internal part).

Figure 11: Force-displacement curves obtained by non-linear incremental analyses.

Figure 12: Deformed shape at collapse of the dome-drum system as a results of the non-linear incremental analyses VD and VHD and associated hinge scheme (displacement scale factor: 50).

Figure 13: Plastic deformation along the direction normal to cracked mortar joints as a results of the non-linear incremental analyses VD and VHD (displacement scale factor: 50).

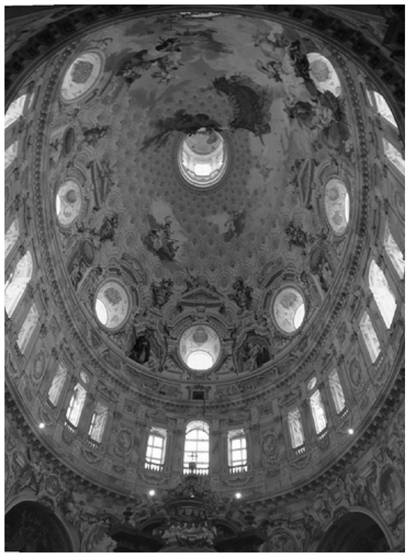

Figure 1: External (left) and internal (right) views of the Sanctuary of Vicoforte.

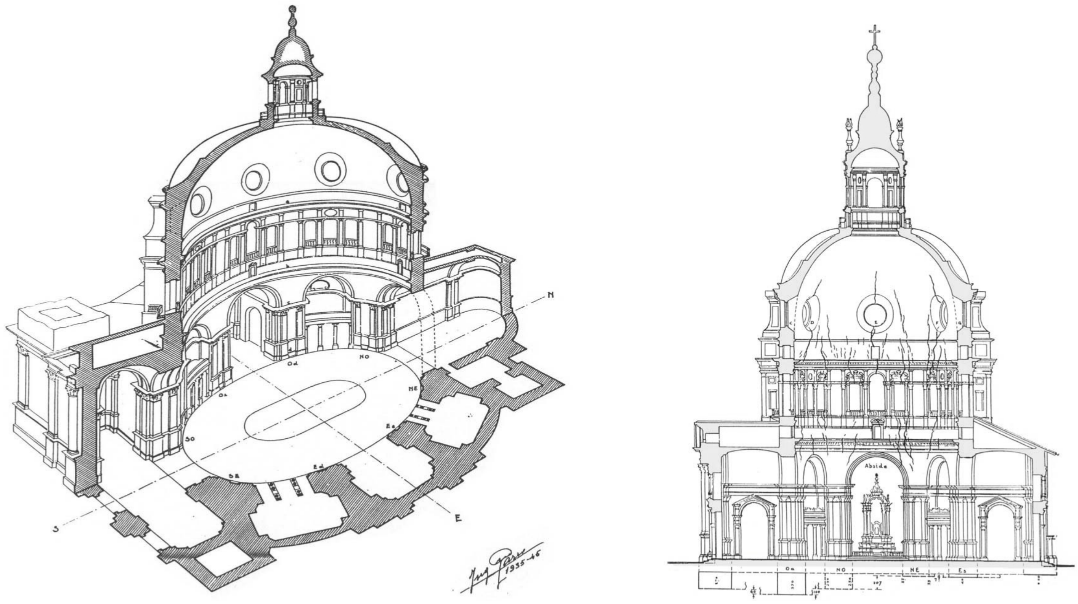

Figure 2: A cross-section of Sanctuary (left) and cracks in the dome (right) of a east-west section, North side view (Garro 1962).

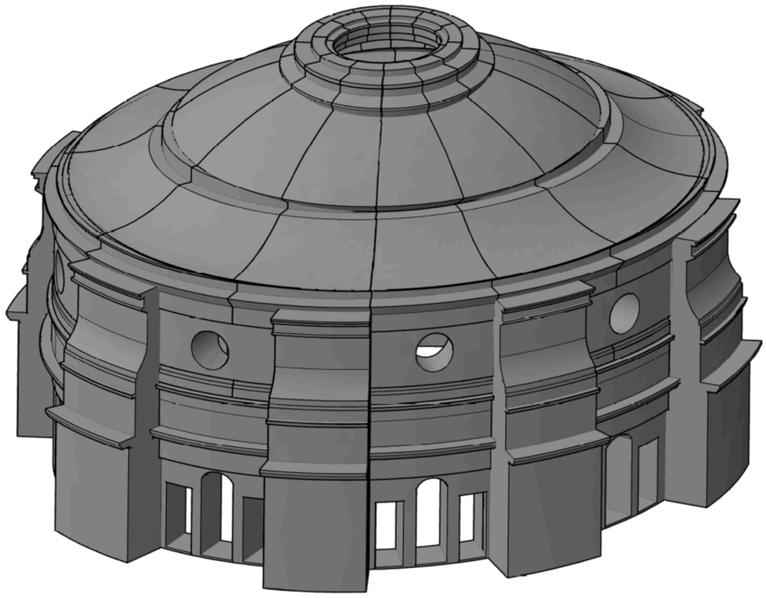

Figure 3: The three-dimensional geometric computational model.

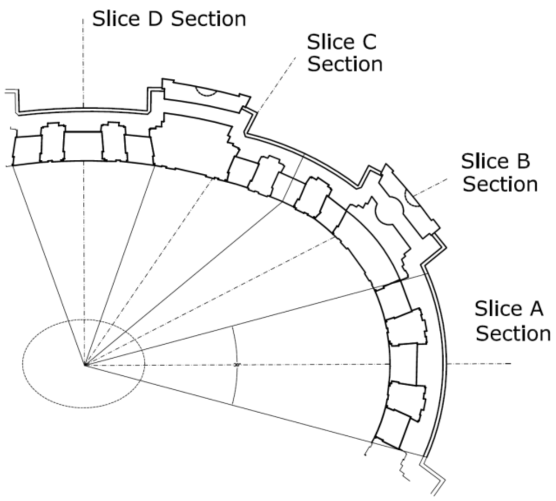

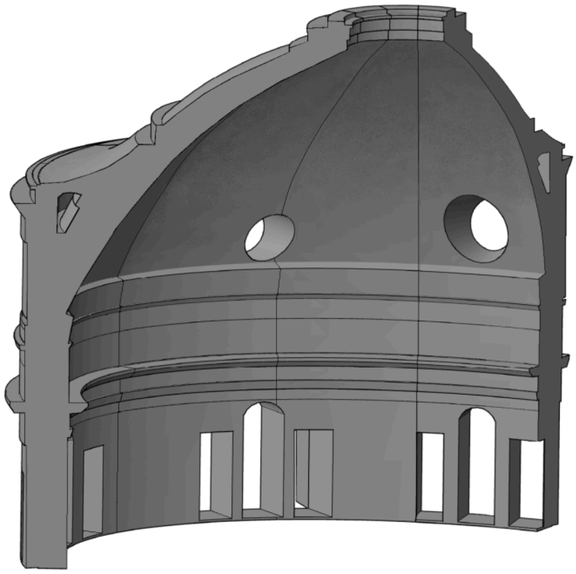

Figure 4: The four fundamental slices. Plan view (left) and 3D view (right).

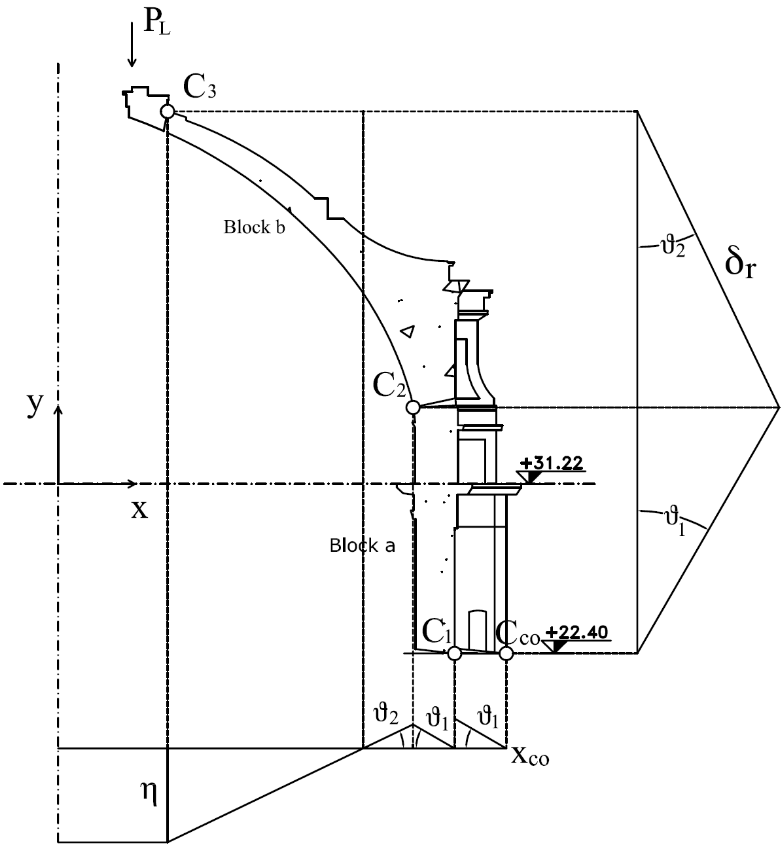

Figure 5: The mechanism in a generic slice.

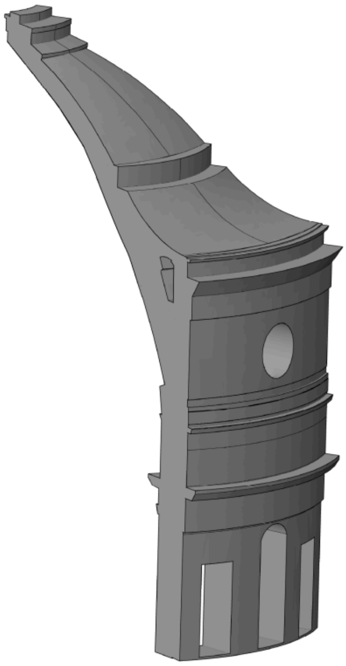

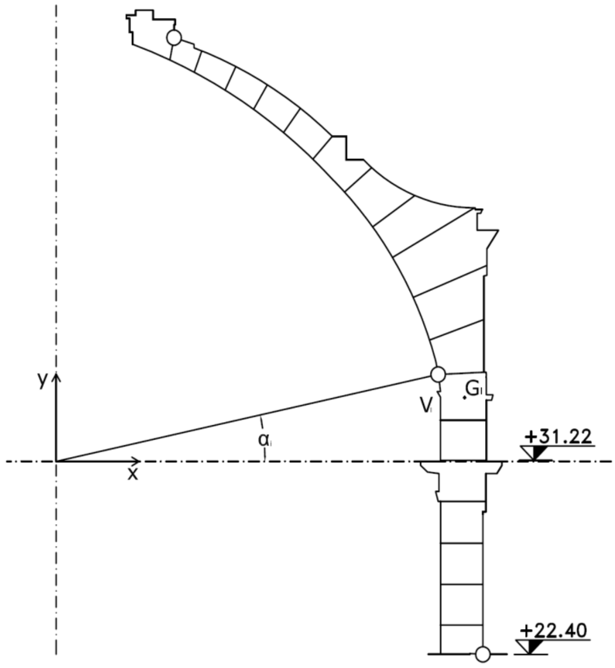

Figure 6: Subdivision of a slice at discrete positions.

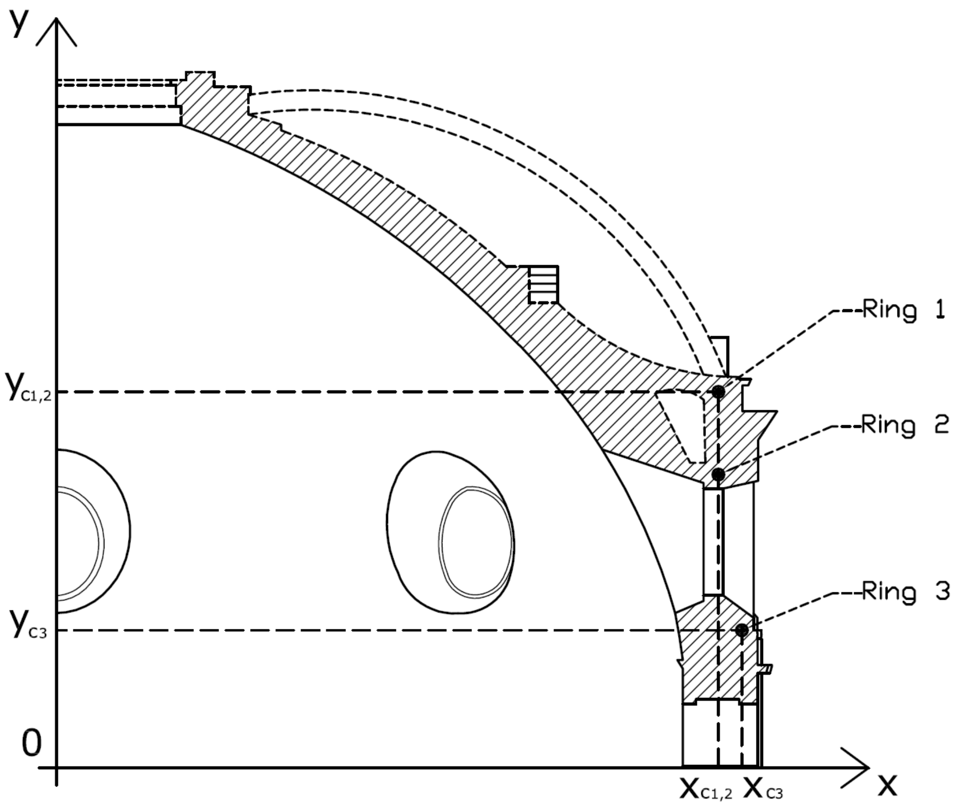

Figure 7: Tension ring positions.

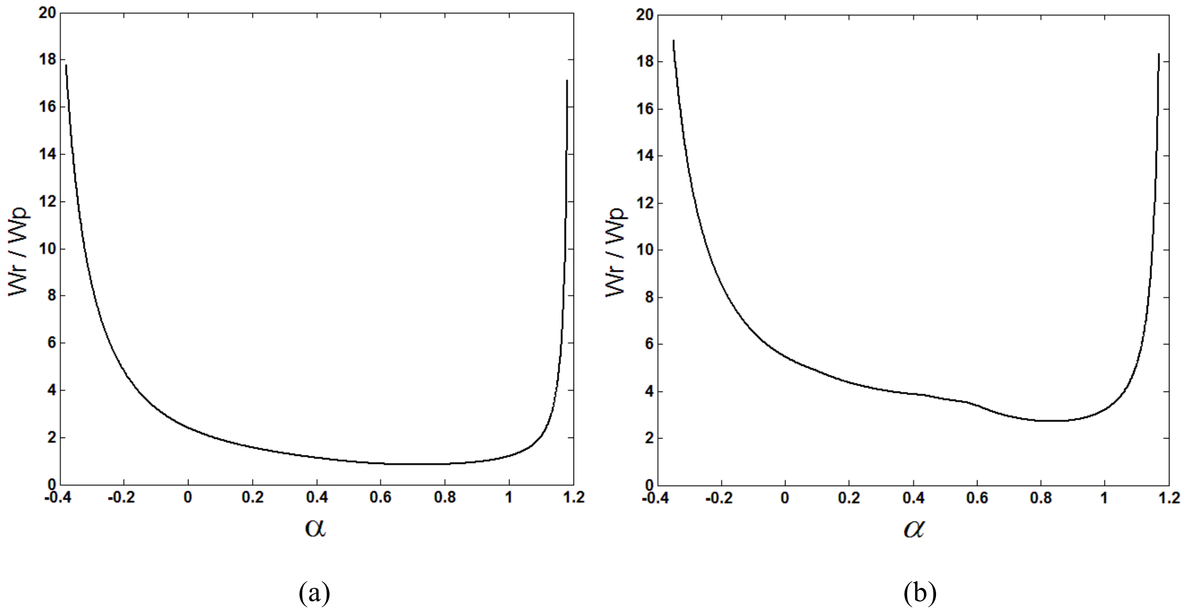

Figure 8: The virtual works ratio vs. intermediate hinge position α in slice A without (a) and including (b) tension rings contribution.

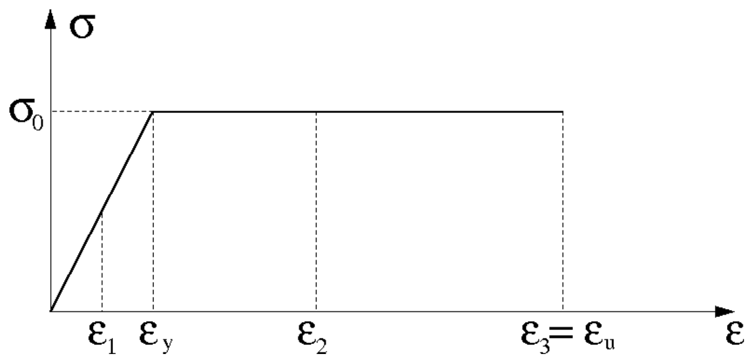

Figure 9: Example illustration of the strain distribution in the tension rings and associated stress state according to elastic-plastic constitutive law.

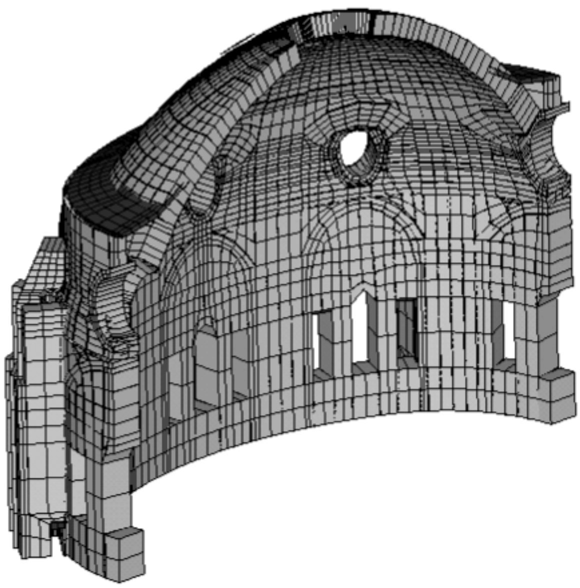

Figure 10: FEM model of the dome-drum system (the model is sliced along the longitudinal axis in order to show its internal part).

VD

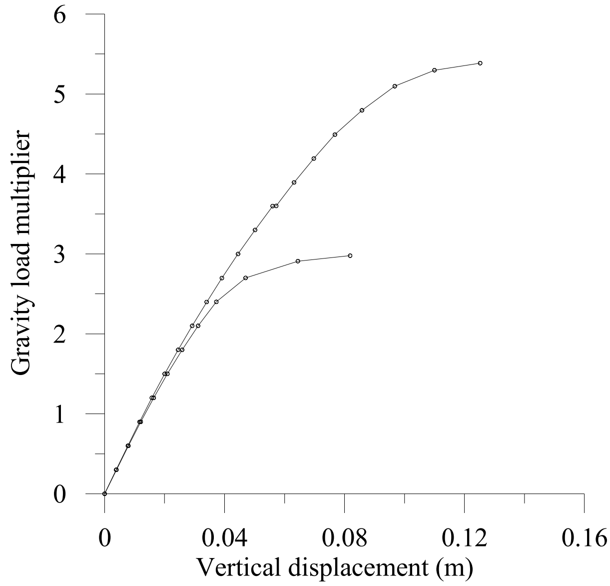

Figure 11: Force-displacement curves obtained by non-linear incremental analyses.

External views

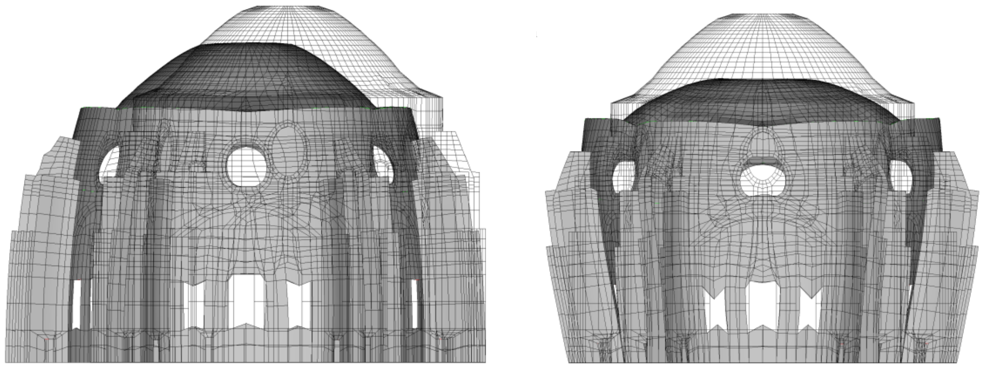

VD VHD

Transversal sections

VD VHD

Hinge schemes

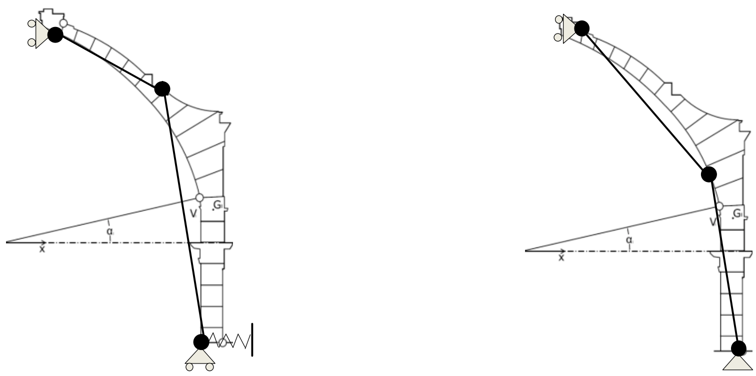

Figure 12: Deformed shape at collapse of the dome-drum system as a results of the non-linear incremental analyses VD and VHD and associated hinge scheme (displacement scale factor: 50).

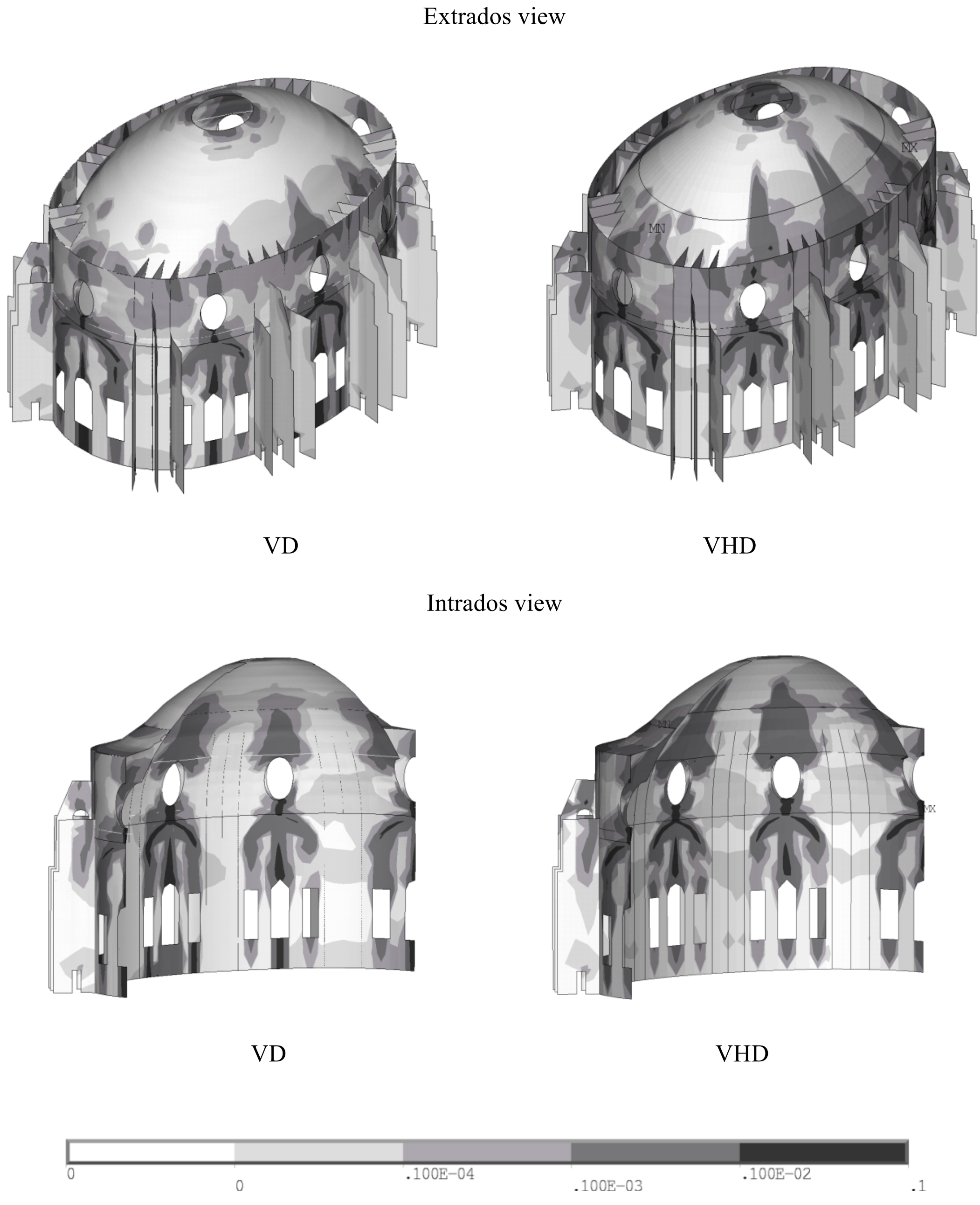

Figure 13: Plastic deformation along the direction normal to cracked mortar joints as a results of the non-linear incremental analyses VD and VHD (displacement scale factor: 50).

LIST OF TABLES

Table 11: Material parameters adopted in the non-linear incremental analyses.

Table 1: Approximating polynomials for center of gravity position of slice blocks.

Center of gravity position X(α [rad]) [m]

Block	**Slice**	**Polynomial coefficients: $c_0 + c_1\alpha + c_2\alpha^2 + c_3\alpha^3 + c_4\alpha^4$**				
		c_0	c_1	c_2	c_3	c_4
C_1-C_2	**A**	+ 19.5110	− 0.7372	− 1.2605	+0.4839	+0.0000
C_1-C_2	**B**	+ 15.1200	+ 0.0191	− 0.5425	− 0.5587	+0.3436
C_1-C_2	**C**	+ 18.2530	− 1.3237	+ 0.6316	−0.5498	+0.0000
C_1-C_2	**D**	+ 13.4600	− 0.2212	−0.5180	+0.0000	+0.0000
C_2-C_3	**A**	+ 16.5390	− 2.6952	− 9.5597	− 7.8945	+ 9.2842
C_2-C_3	**B**	+ 13.1150	− 2.5742	− 4.7658	− 2.1279	+ 2.3035
C_2-C_3	**C**	+ 15.4040	− 3.4865	− 6.4175	− 2.9225	+ 3.5879
C_2-C_3	**D**	+ 11.3270	− 0.8947	− 3.8397	− 3.2862	+ 2.4562

Center of gravity position Y(α [rad]) [m]

Block	**Slice**	**Polynomial coefficients: $c_0 + c_1\alpha + c_2\alpha^2 + c_3\alpha^3 + c_4\alpha^4$**				
		c_0	c_1	c_2	c_3	c_4
C_1-C_2	**A**	− 5.7783	+ 14.9840	− 0.7514	− 11.055	+ 5.1862
C_1-C_2	**B**	− 5.8355	+ 10.3950	− 1.1902	− 3.9220	+ 1.6005
C_1-C_2	**C**	− 5.7953	+ 11.6500	− 0.9111	− 4.5693	+ 1.6352
C_1-C_2	**D**	− 5.7313	+ 8.5582	− 0.3528	− 1.1221	+ 0.0000

C_2-C_3	**A**	+ 6.9589	+ 8.7410	+ 2.0736	− 2.4157	+ 0.0000
C_2-C_3	**B**	+ 6.7750	+ 8.2855	+ 0.8678	− 1.2357	+ 0.0000
C_2-C_3	**C**	+ 7.3693	+ 6.6684	+ 1.0405	+ 3.3287	− 3.0239
C_2-C_3	**D**	+ 7.6597	+ 4.1470	+ 1.7956	+ 4.2010	− 3.1398

Table 2: Approximating polynomials for volume of slice blocks.

Volume V(α [rad]) [m^3]						
Block	**Slice**	**Polynomial coefficients: $c_0 + c_1\alpha + c_2\alpha^2 + c_3\alpha^3 + c_4\alpha^4$**				
		c_0	c_1	c_2	c_3	c_4
C_1-C_2	**A**	+ 186.6700	+ 457.6000	+ 116.1300	−187.0500	+ 0.0000
C_1-C_2	**B**	+ 197.5500	+ 363.3700	+ 2.6555	− 135.3000	+ 39.1070
C_1-C_2	**C**	+ 180.2100	+ 375.5600	+ 39.4010	− 137.8100	+ 22.1320
C_1-C_2	**D**	+ 122.1600	+ 164.6700	+ 29.6310	+ 7.1356	− 28.6440
C_2-C_3	**A**	+ 384.8100	− 539.4900	− 121.5400	+ 420.1800	− 140.5300
C_2-C_3	**B**	+ 283.1200	− 353.2200	− 12.1710	+ 112.9500	− 18.7850
C_2-C_3	**C**	+ 305.2400	− 365.8900	− 46.9350	+ 110.2800	+ 1.7842
C_2-C_3	**D**	+ 189.0300	− 154.2800	− 40.3500	− 26.3950	+ 46.9530

Table 3: Approximating polynomials for intrados curve.

Intrados curve X(α [rad]) [m], Y(α [rad]) [m]						
Curve	**Slice**	**Polynomial coefficients: $c_0 + c_1\alpha + c_2\alpha^2 + c_3\alpha^3 + c_4\alpha^4$**				
		c_0	c_1	c_2	c_3	c_4
X(α)	**A**	+ 18.2570	− 3.7074	− 5.4751	+ 0.0000	+ 0.0000
X(α)	**B**	+ 14.1980	− 1.7757	− 3.3393	− 0.9162	+ 0.0000
X(α)	**C**	+ 17.1300	− 3.2338	− 5.4019	+ 0.2113	+ 0.0000
X(α)	**D**	+ 12.4890	− 0.9033	− 2.4093	− 1.3968	+ 0.0000
Y(α)	**A**	+ 0.0907	+ 18.2740	− 4.8608	+ 0.0000	+ 0.0000
Y(α)	**B**	+ 0.0748	+ 14.0730	− 2.4196	+ 2.0441	− 1.2292
Y(α)	**C**	+ 0.0946	+ 17.1740	− 4.0810	+ 0.3057	− 0.2458
Y(α)	**D**	+ 0.0688	+ 12.3450	− 1.5203	+ 2.5749	− 1.4659

Table 4: Stability results for the dome without tension rings and single independent slices.

Slice	α	$(W_r / W_p)_{Slice}$
A	35° 38’	0.7863
B	41°09’	1.1996
C	44°41’	1.8898
D	41°03’	0.8417

Table 5: Position of the intermediate hinges for the dome without tension rings and global 3D mechanism.

Slice	**α**
A	37°32'
B	41°16'
C	46°54'
D	44°04'

Table 6: Position of the intermediate hinges and stability ratio for the dome with tension rings and independent slices.

Slice	α	$(W_r / W_p)_{Slice}$
A	42°36'	2.7762
B	44°35'	2.9035
C	46°57'	3.5346
D	47°53'	2.6957

Table 7: Position of the intermediate hinges for the dome with tension rings and global 3D mechanism.

Slice	α
A	42°30'
B	44°35'
C	46°54'
D	48°04'

Table 8: Strain in the tension rings for uniform circumferential elongation and ultimate strain at the most strained ring.

Tension ring no.	ε
1	**0.070**
2	0.062
3	0.046

Table 9: Strain in the tension rings for non-uniform circumferential elongation and ultimate strain at the most strained ring segment.

Tension ring no.	Slice A	Slice B	Slice C	Slice D
1	**0.070**	0.058	0.058	0.065
2	0.063	0.051	0.052	0.058
3	0.047	0.034	0.040	0.052

Table 10: Strain and stresses in the tension rings for uniform circumferential elongation and limit elastic strain at the most strained ring.

Tension ring no.	ε	σ (N/mm^2)
1	0.00083	167
2	0.00074	149
3	0.00055	111

Table 11: Material parameters adopted in the non-linear incremental analyses.

Masonry	Mass	Density	1700 kg/m^3
	Elastic parameters	Homogenized normal elastic modulus E_x	2.0 10^3 MPa
		Homogenized normal elastic modulus E_y	1.5 10^3 MPa
		Homogenized tangential elastic modulus G_{xy}	8.0 10^2 MPa
		Poisson coefficient ν	0.2
	Inelastic parameters	Friction coefficient μ	0.6
		Tensile strength of mortar joints σ_{mr}	0.05 MPa
		Cohesion of mortar joints τ_{mr}	0.1 MPa
		Compressive strength of the masonry σ_{Mr}	3 MPa
		Tensile strength of blocks σ_{br}	0.5 MPa
		Shear strength of blocks τ_{br}	2 MPa
		Ratio between the elastic and inelastic shear strain at failure in mortar joints $G_{xy} / \widetilde{G}_{xy}$	2
		Ratio between elastic and inelastic strain in the masonry in compression at failure $E_y / \widetilde{E}_y$	1.5
		Softening coefficient of mortar joints β_m	0.2
		Softening coefficient of blocks β_b	0.2
		Interlocking ratio φ	4
Rings	Elastic parameters	Elastic modulus E	200000 MPa
		Poisson modulus	0.2
	Inelastic parameters	Strength	167 MPa